International Journal of Mechanical Sciences 244 (2023) 108029

Contents lists available at ScienceDirect

International Journal of Mechanical Sciences

journal homepage: www.elsevier.com/locate/ijmecsci

Inverse machine learning discovered metamaterials with record high recovery stress

Adithya Challapalli, John Konlan, Guoqiang Li *

Department of Mechanical and Industrial Engineering, Louisiana State University, Baton Rouge, LA 70803, USA

ARTICLE INFO

Keywords:
Metamaterials
Cellular structures
Lattice structures
Machine learning
Shape memory polymer

ABSTRACT

Lightweight shape memory polymer (SMP) metamaterials integrated with high strength, high flexibility, and high recovery stress are highly desired in load carrying structures and devices. A grand challenge is that these desired properties have contradictory requirements, for instance between strength and flexibility, and between flexibility and recovery stress. In this study, an inverse design framework using statistical tools and machine learning models is developed to design thin-walled cellular structures with the desired properties. The discovered thin-walled cellular structures are 3D printed using a novel SMP, which exhibited excellent structural properties with record high specific recovery stress. For comparison purpose, lattice structures discovered previously are also 3D printed using the same SMP. The density normalized recovery stress of the validated lattice unit cells is 30% higher than that of the Octet lattice unit cell. The optimal thin-walled unit cells exhibit exponentially higher recovery stress than the honeycomb unit cell in the in-plane orientation and 50% higher recovery stress than other thin-walled structures (both unit cells and 4 × 4 structures). As compared to the solid SMP cylinders, the thin-walled unit cells exhibit 200% higher normalized recovery stress. The inverse design framework can be applied for structural optimization of various other designs and applications.

1. Introduction

Since the concept of 4D printing was coined in 2013 [1,2], shape memory polymers (SMPs) have found ever-increasing applications in many engineering sectors. Volumetric printing can further increase the printing speed of SMPs [3,4]. While excellent shape recovery is one of the selling points for 4D printed SMP structures, stress recovery is highly desired for some applications, for example, serving as actuators in deployable structures [5,6] and as crack closing device in damage self-healing per the close-then-heal (CTH) strategy [7,8]. Several studies have been focused on exploring different techniques to enhance the shape memory properties of SMPs. A blend of PLA (Polylactic acid) and TPU (Thermoplastic Polyurethane) were studied at different temperatures to improve the shape memory effect of PLA. It is observed that the preformation temperatures have significantly positive effect on the recovery stress of the PLA and TPU blend [9]. The effects of cold and hot temperatures on the SME (shape memory effect) of a novel PETG (poly-ethylene terephthalate glycol) polymer were also studied, suggesting that hot programing exhibits higher recovery stress [10]. Other studies such as using nanocomposite [11,12] or using enthalpy as the energy storage mechanism [13,14] have also been conducted to enhance the recovery stress. However, the room for further growth is small because high recovery stress requires high stiffness in rubbery state, which reduces the shape or strain recovery. Therefore, design and discovery of new SMPs with high load carrying capacity, high strain recovery efficiency, and high recovery stress remain a grand challenge.

It is noted that, in the open literatures, most reported recovery stress values are based on test results of solid samples such as cubes or cylinders, with only a few exceptions that examine lattice structures [15,16]. It is well-known that if a material is manufactured into various structures, its specific load carrying capacity can be significantly enhanced, for example, I-beams, T-beams, box-beams, sandwich beams, instead of solid cuboid beams. Therefore, it is expected that if SMPs are 3D printed into metamaterials, the specific recovery stress can be enhanced as compared to solid SMP structures.

Lightweight metamaterials refer to structures such as lattice structures, thin-walled cellular structures, auxetic structures and hybrid plate-lattice cells. These structures have been widely studied due to their multifunctional advantages in structural, acoustic, and thermal applications. Numerous studies have been focused on proposing theoretical

* Corresponding author.
E-mail address: lguoqi1@lsu.edu (G. Li).

https://doi.org/10.1016/j.ijmecsci.2022.108029
Received 20 October 2022; Received in revised form 15 November 2022; Accepted 10 December 2022
Available online 16 December 2022

models to predict and analyze the structural behavior of the metamaterials [17–21]. Previously, mechanically tunable metamaterials using Octet and Kelvin lattice unit cells were 3D printed using a shape memory polymer (SMP) [22]. Auxetic structures with tunable mechanical properties were designed and 3D printed using SMPs that can be used in medical devices [23]. A hierarchically structured metamaterial with strain-dependent solid–solid phase change was designed with applications in micro-actuators and grippers, and programmable device [24]. Several other two-dimensional and three-dimensional auxetic structures have been proposed so far by comparing their mass, buckling load, natural frequency, Poisson's ratio, and compression strength with abundant numerical and experimental results [25]. The unique behavior of auxetic structures due to their structural orientation has several applications in medical, sport, and automobile devices [26]. Topology optimization techniques were mostly used to optimize these metamaterials to achieve maximum performance [27]. One disadvantage of topology optimization is that it can only optimize structures based on a single parent design, while there is an extensive design space for the global optima. To overcome this limitation, several data driven structural design and optimization techniques were proposed to design novel metamaterials. Inverse design frameworks using Generative Adversarial Networks (GANs) and machine learning regression models were proposed to explore a wide range of design space towards the global optima [21].

Machine learning tools learn from a training dataset to identify hidden patterns which can be used for the classification or prediction of untrained dataset with minimal human interaction and computational power. Machine learning and data analytical frameworks were extensively explored for the discovery and optimization of several new materials, structures, and systems [28–31]. Machine learning tools were shown to surpass the complex trail-and-error process for experimental or computational analysis in discovering new porous crystalline materials such as zeolites and metal organic frameworks [29]. A hybrid structural design and optimization model was developed to optimize wind turbines that were proven to have identical accuracies compared to complex Computational Fluid Dynamics (CFD) simulations [30]. Gradient and no-gradient based automatic machine learning optimization loops were developed to design multifunctional metamaterials to accelerate the design of complex devices for communication, computing and optical device applications which otherwise were unachievable with conventional physics-based approaches [31]. Previously, we reported several novel lightweight metamaterials with superior compression strengths, buckling loads, higher natural frequencies, and better impact energy absorptions [21,32,33]. Though a few structures were predicted with decent shape memory properties, only few structural selection or optimization methods have been explored so far. The numerical evaluation for the SMP metamaterials can be overly complex due to their unique thermomechanical behaviors, and the experimental validation is time taking due to the multi-step thermomechanical procedures, especially when complex structures are involved.

In this paper, a simple design criterion to discover optimized metamaterials with superior shape memory properties are proposed. For optimal shape memory performance, a structure should be flexible to be able to have larger displacements (pre-strain) during programming, and strong at the same time to store higher programing stress. To balance these two contradictory requirements within the lightweight structures, we started by considering bending-dominated structures. Bending-dominated structures have been shown to have high flexibility [34,35], which satisfies the requirement for larger displacement. Periodic hexagonal honeycomb structures were studied for their in-plane high shear strength and shear strain with applications in passive morphing airfoil [36]. Now by optimizing bending-dominated structures with superior strength or larger programming stress, it satisfies the second requirement. As a result, bending-dominated structures with high strength could lead to superior recovery stress. To this end, design spaces for 3D bending-dominated lattice unit cells and thin-walled cellular unit cells are explored to identify optimal structures with superior strength and recovery stress properties. While stretch-dominated lattice structures and thin-walled cellular structures with very low relative density can exhibit large deformation through buckling, we do not consider this type of structures because they do not satisfy the requirement for high programming load.

Previously, while several thin-walled unit cells with superior strength and auxetic properties have already been proposed, there is a research gap in proposing techniques to explore a wide range of design space. While techniques like topology optimization can lead to optimal structures, a data driven technique can be much closer to the global optima [20,21]. In this paper, a novel design optimization framework using existing supervised machine learning regression models and statistical analysis techniques is proposed to discover novel optimized thin-walled cellular structures with superior strength and recovery stress. While the models used in this study were widely used in various studies, up to our knowledge the combination of these techniques for structural optimization has not been proposed so far. For comparison purpose, the optimal 3D lattice unit cells were adopted from our previous studies where we used machine learning regression models and GANs to optimize them with respect to uni-axial and multi-axial strengths [33]. Maxwell's criterion for rigidity of frames is used to select optimal bending-dominated lattice unit cells. This criterion with few assumptions is then extended to the thin-walled cellular structures for unit cell classification and selection. Numerical and experimental comparisons are performed to validate the proposed inverse design framework and optimal structures. Both bending-dominated lattice unit cells and thin-walled cellular unit cells demonstrate high strength, good flexibility, and record high recovery stress.

2. Thin-walled cellular structures

Thin-walled cellular structures can be presumed as a combination of several thin-walls in different orientations. In this section, a brief review on thin-walled structures is presented, followed by numerical comparisons of thin-walled unit cells in different orientations and lattice unit cells. Lastly, the motivation for this study and the steps implemented for the optimization of these unit cells are also discussed.

Regular thin-walled cellular structures such as honeycomb have excellent strength and shock absorption properties due to their lightweight and effective mechanical properties [17]. They have several industrial applications such as in automobiles, aircrafts, naval vessels, etc. Various studies have been focused on developing new techniques to design, optimize and manufacture these lightweight structures and expand their applications [37–42]. With the advancement in complex analyzing tools and additive manufacturing technologies, research advancements in the design of these structures have become quite rapid [38]. Based on plastic deformation of metals, a new platform to design flexible and programable crashworthiness thin-walled structures was proposed which produced thin-walled structures that exhibit 54% higher specific energy absorption properties [39]. Unit cells with multi-level configuration that have higher degree of freedom were proposed with applications in reconfigurable structures [40]. Apart from exceptional mechanical properties, the thin-walled unit cells were explored for their application in broadband microwave absorption, acoustic insulation, etc. An evolutionary optimization (EO) based program was developed to optimize honeycomb unit cells with mechanical-electromagnetic property integration [41]. Also, honeycomb structures were optimized to achieve low frequency sound transmission loss that was greater than 45 dB [42]. Multiscale topology optimization techniques were proposed to design inhomogeneous cellular structures with higher natural frequencies [43]. Hierarchical thin-walled structures were investigated for their energy absorption properties, and it was found that higher-order cellular structures enhanced these properties [44]. Numerical and experimental validation techniques were proposed to investigate the potential of honeycomb

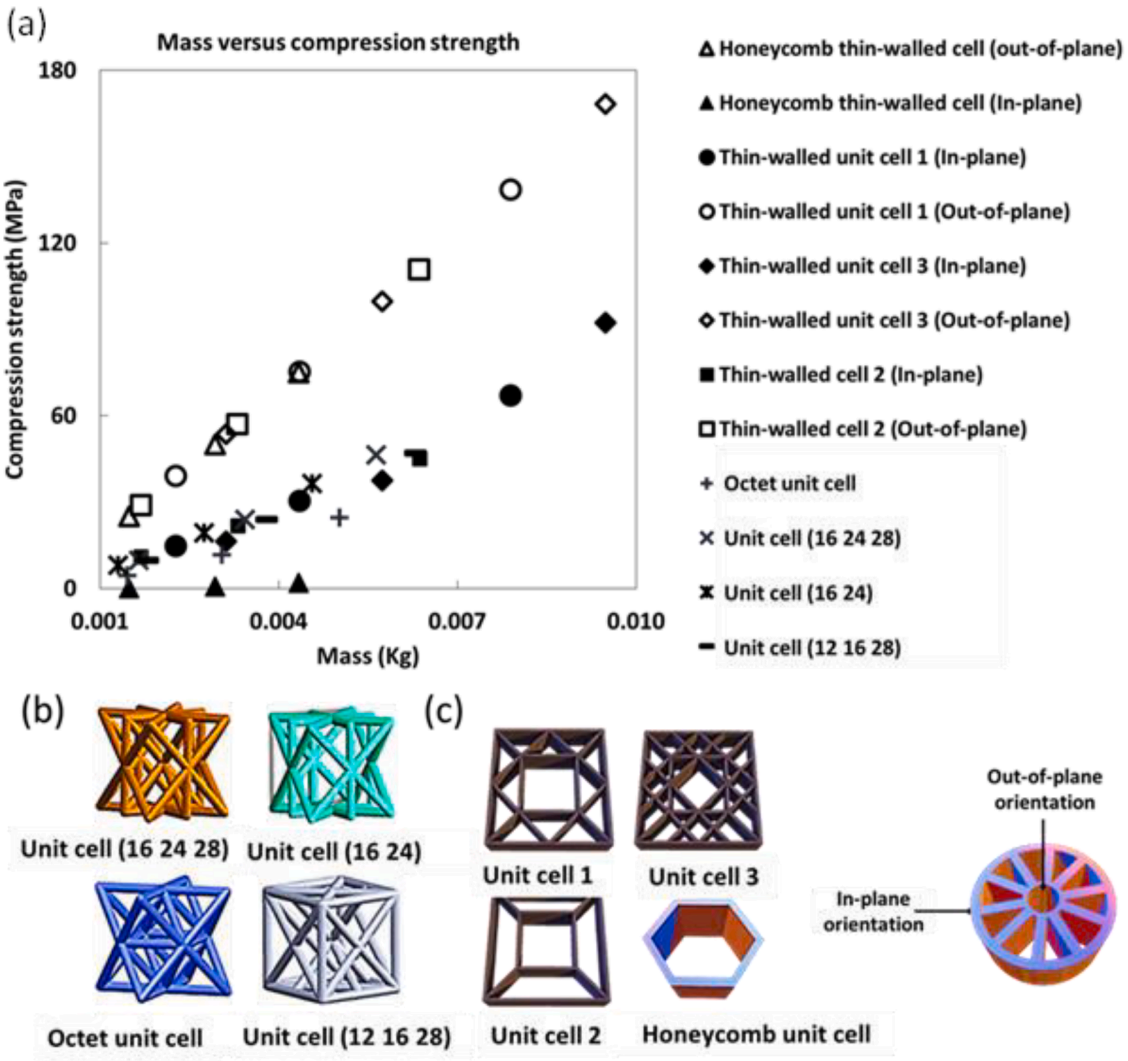

Fig. 1. (a) Numerical comparisons of various lattice and thin-walled cellular structures (in-plane and out-of-plane) under uni-axial compression with increase in mass as a function of truss diameter or thin-wall thickness using ANSYS simulations, (b) lattice unit cells and (c) thin-walled unit cells. All the unit cells are designed with the same overall volume and varying rod diameters and wall thicknesses. (a) shows that the compression strength of all the unit cells increases with rod diameter and wall thickness. Especially, while lattice unit cells and thin-walled unit cells in the in-plane orientation have similar strengths, thin-walled unit cells in the out-of-plane orientation exhibit superior strength over similar mass range.

structures to store thermal energy and it was observed that such structures significantly improved the efficiency of operation of ultra-high temperature systems [45]. The vehicle handling and cushioning effect of non-pneumatic tires were enhanced using various types of honeycomb unit cells [46]. In an earlier study, we proposed several thin-walled unit cells with compression strength 50–250% and impact strength 300% higher than the conventional honeycomb unit cell in the out-of-plane orientation without considering the in-plane structural properties using generative adversarial networks (GAN) (Refer to Table S6 for parameters in the GAN system) [21].

Compared to lattice structures such as the Octet lattice, the thin-walled cellular structures exhibit higher compression strengths in the out-of-plane orientation, but weak in-plane or lateral orientations as seen in Fig. 1. This can be easily comprehended by observing the orientation of the cellular walls in different thin-walled structures. While all the walls primarily contribute to the compression strength in the out-of-plane orientation, only certain walls contribute to the strength in the in-plane orientation. One structural advantage of in-plane orientation of the thin-walled structures is the mode of deformation. Under compression load, the thin-walled structures fail due to wall bending or buckling. While buckling could lead to catastrophic failure, bending is not as bad. Wall bending could aid in higher flexibility, better recovery stresses and better structural packing ability. Especially, the in-plane orientation of a thin-walled cellular structure has a wider range of flexibility due to the multiple orientations of the cell walls.

Fig. 1 shows the comparisons of several lattice unit cells [18] and thin-walled cellular structures in both in-plane and out-of-plane orientations with respect to compression yield strength. It can be observed that the thin-walled unit cells in the in-plane orientation have much lower strengths compared to their out-of-plane orientation but still in par with lattice unit cells. The porous nature of thin-walled unit cells and the mode of deformation of wall elements in the in-plane orientation also suggests that the thin-walled structures can have higher displacements in the in-plane orientation, leading to applications in areas such as energy absorption, impact tolerance and higher shape recovery properties.

To study the thin-walled structural performance in the in-plane orientation and optimize them for superior stress recovery properties, the following steps are followed. Firstly, to explore a larger space of structural design, a dataset of possible thin-walled cellular structures within a design space shall be formed using a representative volume element (RVE). Secondly, machine learning regression models using a

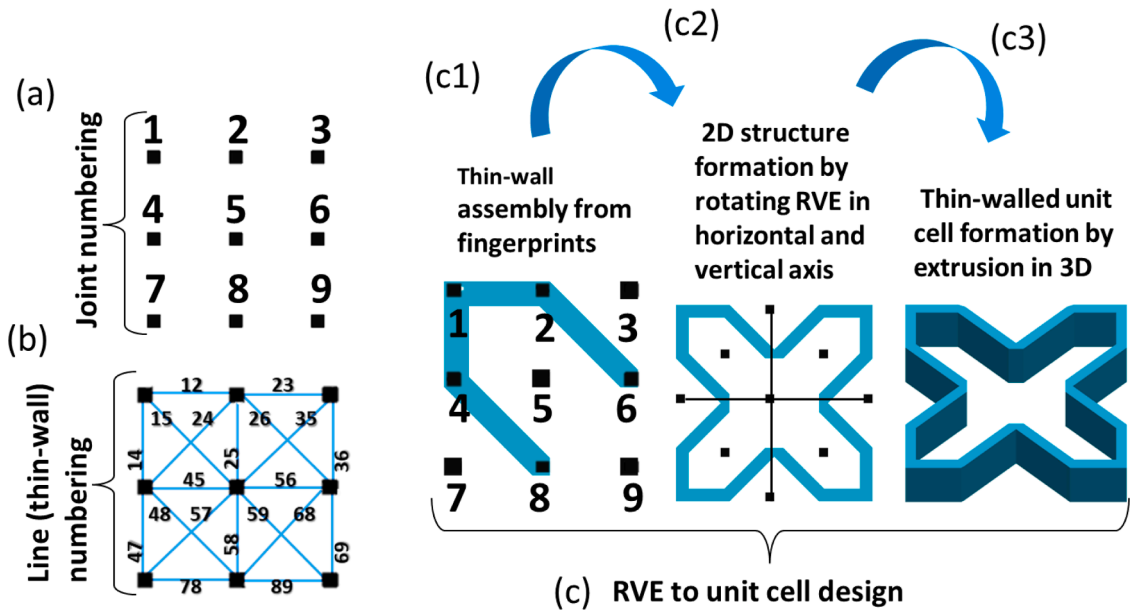

Fig. 2. Representative volume element (RVE) for the thin-walled unit cells. (a) The RVE consists of 9 joints that can be used to form a total of 20 lines (thin walls). (b) By connecting the neighboring points, a total of 20 lines (thin walls) can be formed. Any of the two numbers in a line is a fingerprint of that line. (c) Procedure from the RVE to unit cell: (c1) collect the fingerprints of the lines in (b) in vector format to form a quarter of a unit cell, for example (12 14 26 48); (c2) mirror the quarter unit cell in vertical and horizontal axes to form a symmetric 2D unit cell; (c3) extrude the 2D unit cell in the out-of-plane direction to create a 3D unit cell.

training dataset that can predict the structural properties of any unit cell within the RVE shall be developed. The machine learning regression models assist in drastically reducing the property prediction time and computational power. Thirdly, a design criterion to differentiate the unit cells based on their structural behavior (i.e., bending-dominated, or stretching-dominated) shall be proposed. Finally, an inverse design framework using the machine learning regression models and statistical analysis tools shall be assembled to predict novel lightweight structures with superior strength and recovery stress.

3. Materials and methods

In this Section, the techniques used to generate and prepare the training data sets for machine learning models to predict the mechanical properties such as mass and compression strength are thoroughly discussed in Section 3.1. Section 3.2 discusses the applications and implementation of the machine learning regression models. In Section 3.3, the criterion to select flexible lightweight structures using Maxwell's criterion is discussed. The inverse design framework proposed by a combination of the correlation analysis, machine learning regression models and the selection criterion is presented in Section 3.4. Finally, in Section 3.5, the numerical and experimental validations are reported by testing 3D printed thin-walled cellular structures and lattice structures using a shape memory polymer (SMP) ink.

3.1. Dataset generation and fingerprinting for thin-walled cellular structures

Machine learning models and statistical analysis tools require a minimum size of training data for optimal performance. The size of the training dataset primarily depends on the input and output variables. As the number of independent variables that affect the outputs increases, the data size required to train a decent model also gets bigger. In this section, we present the methods used to generate the training dataset for predicting the structural properties of thin-walled structures along with the fingerprinting technique.

To explore a wide range of novel structural designs, certain boundary conditions should be set such that a large variety of unexplored design space with extensive structural properties can be covered without making the optimization task too complex. For this purpose, a representative volume element (RVE) with 9 points (joints in 3D) is considered as shown in Fig. 2. A total of 20 lines (thin walls in 3D) can be formed by connecting every two adjacent points. Here for simplicity, only the nearest neighboring points are connected to form a line. For example, points 1 and 2 can be connected to form the line (12), but 1 and 3 cannot be connected as there is a point (point 2) in between them. Similarly, with various combinations of these lines and by mirroring the RVE into the horizontal and vertical axis for each combination, a huge dataset of nearly a million different thin-walled structures can be obtained. It is noted that if we allow connection of non-nearest neighboring points such as 18, 19, a total of 35 lines will be created, which will lead to a much larger training dataset, and may capture more optimized structures. For simplicity and for demonstrating the machine learning framework only, we used 20 lines in this study.

To train a machine learning algorithm (supervised), it should be provided with a training dataset containing both the inputs, which are the structures, and the outputs, which are the desired mechanical properties of each structure. The structures must be fingerprinted for the machine learning algorithm to interpret the data. Fingerprinting is the process of converting each structure into a machine-readable logical sequence or pattern of digits. In this study, each structure is initially named with the combination of all the joints forming that particular unit cell within the RVE. For example, the thin-walled structure in Fig. 2 is fingerprinted as (12 14 26 48), where (12) represents the line or wall formed by connecting points (joints) 1 and 2. Similarly (14), (26) and (48) represents lines or walls connecting points 1 and 4, 2 and 6, and 4 and 8, respectively. Since the position of the joints and their digital representations are fixed, each structure formed within the RVE can be given a unique logical fingerprint (Refer to Fig. S6 for sample structures and fingerprints). This procedure can be easily followed to convert any structure into a fingerprint and vice versa. For the machine learning regression training, these fingerprints are further converted into a binary format which improves the prediction accuracy. This is done by assigning a fixed position for each formed line in a vector and by representing all the line positions present in a particular structure with 1′s and the rest as 0′s in the vector. In this study, the line 12 is assigned the

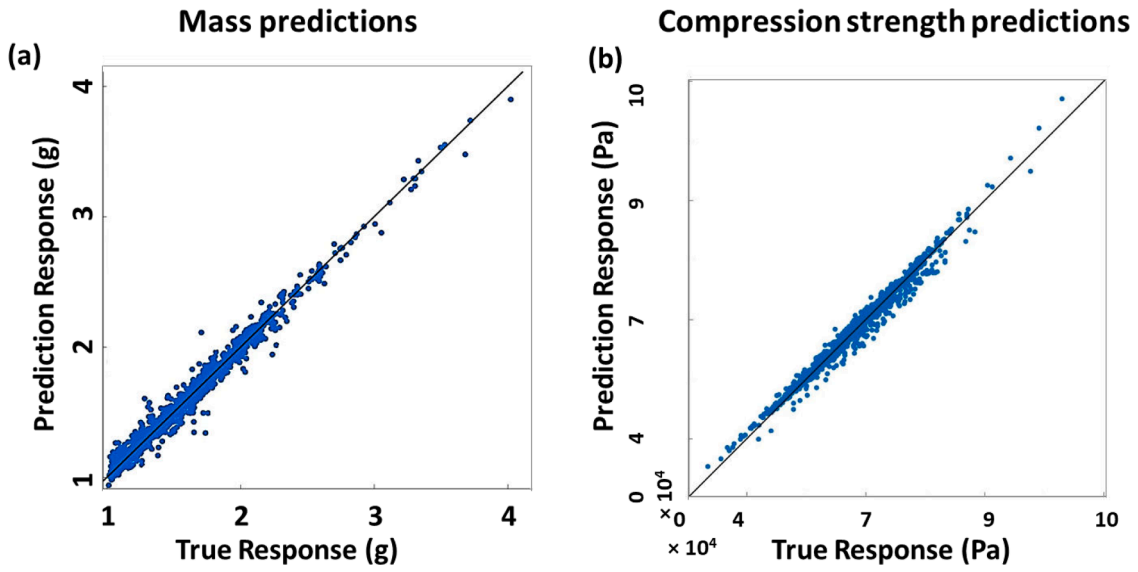

Fig. 3. Gaussian Process Regression (GPR) models for (a) mass and (b) compressive strength predictions. A training dataset of 2000 fingerprints is used to train the GPR model, and the prediction accuracy R-squared value is 0.98. The blue dots (•) represent the observations, and the inclined solid lines represent perfect predictions. The roughly even scattering of the observation along the perfect predictions represents a solid regression model.

1st position in the binary format vector and similarly, 14, 26 and 48 are given the 7th, 15th, and 17th positions in the vector. Hence the fingerprint of the cellular structure in Fig. 2 will be represented in the binary format as (1 0 0 0 0 0 1 0 0 0 0 0 0 0 1 0 1 0 0 0). While all the unit cells formed using the proposed RVE will be unique to one another, some structures will be repetitive if tessellated to form an infinite lattice. For example, unit cells (15 59 89 78 47 14) and (35 57 78 89 69 36) will form the same lattice structures when tessellated (Refer to Fig. S6 for the two unit cells). Since this study is focused on optimizing the unit cells only, the repetitive fingerprints (if tessellated to form an infinite lattice) were ignored. This facilitates the ease of data handling and data generating processes. However, if one is to use the RVE to create lattice structures by tessellation, attention must be paid to the possibility that different unit cells may create the same lattice structure.

In this study, all the structures are fingerprinted using the above stated procedure. MATLAB combination function is used to generate a dataset of all possible structures within the RVE using simple coding. A training dataset of 2000 fingerprints is extracted randomly from the untrained dataset for the machine learning regression analysis. MATLAB functions such as "y = datasample(data,k)" are used for the training dataset extraction.

3.2. Forward machine learning prediction

The main motivation for this study is to predict optimal thin-walled structures with superior recovery stress. As discussed earlier, directly calibrating the shape memory effect or the recovery stress of these structures is a complex and time-consuming procedure, both experimentally and numerically [47,48]. The experimental analysis involves structure manufacturing, experimental setup and a multi-phase shape memory training, which is extremely time consuming, especially when multiple samples are involved. The numerical analysis can also be very complex as it involves many curve-fitting parameters, non-linear material properties and thermomechanical analysis [49–51]. Since the training dataset is comparatively large, it is impossible to adopt any of the above conventional procedures.

For this purpose, as this is a structural optimization problem, if the material properties, overall volume, and test boundary conditions for all the structures are kept the same, the overall recovery stress of a structure will depend on the energy stored during programming and the total strain stored. For a given SMP, its recovery stress depends on the programming strain only because the shape fixity ratio, shape recovery ratio, and rubbery modulus are SMP-dependent only. In other words, higher displacement will lead to higher strain, and thus higher energy storage and better recovery stress [52]. The maximum displacement occurs when the structure or a structure element fails. Hence, under uniaxial compression, the compression strengths of all the structures in the training dataset are recorded along with their masses. ANSYS simulation software is used to model (Workbench design modeler) and evaluate all the 2000 thin-walled structures. The data generation is performed on a workstation with 32 GB RAM, i7 processor and the total computational time for the training dataset is about 75 to 85 man-hours. Mesh convergence analysis is conducted for consistent results (Refer to Fig. S2 for details). The numerical analysis is performed by considering only the elastic properties of the base material to minimize complexities and time consumption that might rise if the viscoelastic properties are considered. Once a material is selected, the recovery stress of the structures depends on their programable strain which is governed by the number of elements and their orientations. Therefore, the model should be applicable irrespective of the material properties. Once the training dataset is ready with the input fingerprints and the output mass and compression strength properties, MATLAB Regression Analysis tool is used to compare several machine learning algorithms for their prediction accuracies with the training dataset. With a five-fold validation, the Gaussian Process Regression (GPR) model outperformed other machine learning models such as ensemble tree and Support Vector Machines (SVM) with a root mean square error (RMSE) less than 5% and R-squared value of 0.98 for both the mass and compression strength properties; see Fig. 3 (Refer to Tables S2 (a) and S2(b) for model parameters and comparisons). The GPR model is a kernel based probabilistic model which uses a set of random variables having a Gaussian distribution to do the predictions [21]. Previously, the GPR models were proven to work best compared to other models for supervised machine learning regression models, especially with structural data and their mechanical property predictions.

3.3. Selection criterion for optimal structures

Once the suitable machine learning models are selected, it can be used to predict the structural properties for the rest of the designs from the entire dataset within a few minutes and with minimal computational power. Now the first requisite for optimal recovery stress, i.e., the

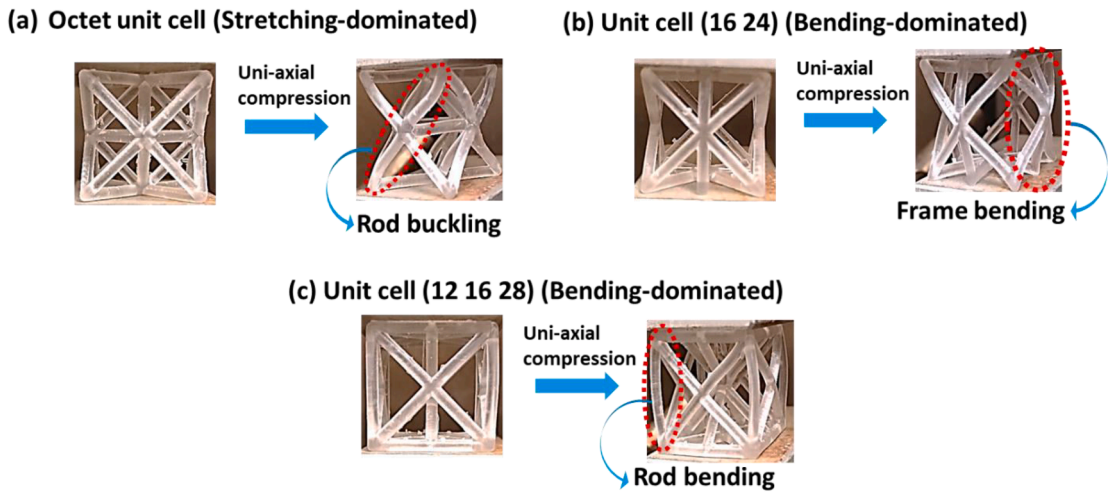

Fig. 4. Behavior of stretching-dominated and bending-dominated lattice unit cells under uni-axial compression. (a) Octet unit cell, (b) Unit cell (16 24), and (c) Unit cell (12 16 28). The Octet unit cell can be observed to display a stretching-dominated behavior with local rod buckling, but the proposed bending-dominated unit cells display a global or local rod bending behavior. It is noted that during test, if bending occurs suddenly, we define it as buckling; if bending grows with load, we define it as bending-dominated structure.

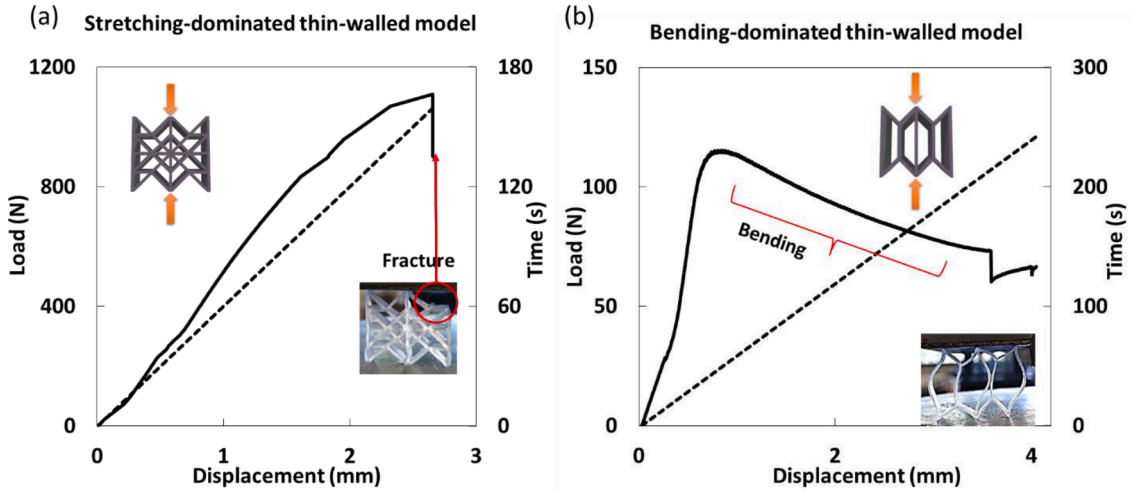

Fig. 5. Experimental load vs displacement (solid curve) comparisons over time (dotted line) under uniaxial compression for (a) Stretching-dominated unit cell, and (b) Bending-dominated thin-walled unit cell. The solid lines represent load vs displacement, and the dotted lines represents displacement vs time comparisons. The bending dominated unit cell (b) can be observed to show lower load bearing capacities, higher displacements, and flexible deformation behavior in the in-plane direction compared to the stretching dominated unit cell (a). It can also be seen that the unit cell in (b) requires longer time before failure (300 s), supporting the bending like behavior; and the unit cell in (a) requires less time before failure, representing stretching like behavior. Furthermore, it is seen in (a) that the load dropped suddenly, suggesting fracture of some rods; while the load drops gradually in (b), suggesting bending.

compressive strength of any structure within the specified design space can be calibrated using the regression model. The second requisite, which is the maximum displacement of a structure before failure is also crucial for optimal recovery stress. For this purpose, the study of lattice structures and their behavior based on the number of the elements and joints shall be referred. In general, when a lattice structure is under axial loading, the elements or rods carry the load. Based on the Maxwell's criterion for rigidity of frames Eqs. (1) and ((2)), the lattice structures can be either stretching-dominated or bending-dominated [37,38]. It is noted that Maxwell's criterion was originally for pin-jointed structures. 3D printed joints are, generally speaking, not pin joints. Furthermore, there are well-known exceptions to the criterion, and buckling muddies Ashby's original intent in using the criterion. Recently, some researchers have extended Maxwell's criterion to 3D printed structures which have elastic or rigid or frozen joints [51–54]. In this study, we used Maxwell's criterion as a rough guide to help us select bending- or stretching-dominated unit cells.

$$M = b - 2j + 3, 2D \ structures(frames) \tag{1}$$

$$M = b - 3j + 6, 3D \, structures \tag{2}$$

where b is the number of truss members, and j is the number of frictionless joints. Here if $M \geq 0$, the structure is stretching-dominated and if $M < 0$, the structure is bending-dominated.

In stretching-dominated structures, the mode of failure is due to the rod stretching or buckling while the bending dominated structures fail primarily due to the rod bending. Thus far, several reports have suggested that stretching-dominated structures have higher strength and toughness as compared to their bending-dominated counterparts due to the rigidity in the framework [35,55–57]. In our previous studies [20], we reported several novel lattice unit cells with superior compression strength properties compared to the classical Octet lattice unit cell.

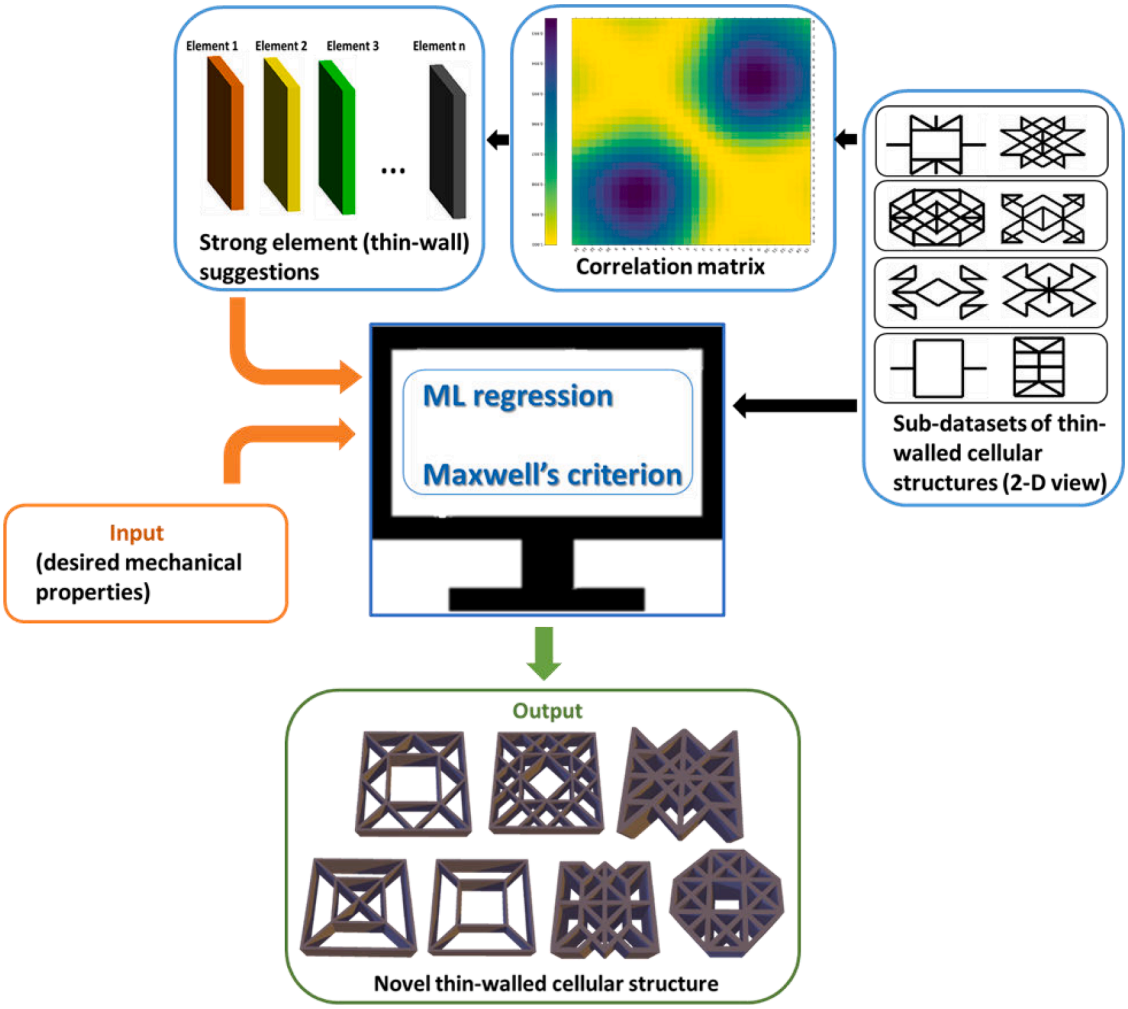

Fig. 6. Inverse design framework for thin-walled structural optimization. The inverse design framework is formed by combining the ML regression models, correlation analysis and the selection criterion. First the machine learning regression models were trained using a training dataset to predict the mechanical properties of the thin-walled unit cells. The inverse design framework is later formed by applying correlation analysis to generate new designs with optimal strength and then extract flexible structures by applying Maxwell's criterion. Hence, the input for the framework will be the desired mechanical properties and output will be optimal flexible and strong thin-walled unit cells (Refer to Fig. S7 for flowchart representation).

However, we did not print the structures with SMP and did not explore their recovery stress properties. Up on further investigation, contrary to the literature up to now, it is observed that several of the optimal structures, which are bending-dominated, exhibit similarly or even higher relative compression strength compared to their stretching-dominated counterparts. In our previous study [20], we considered a RVE with 27 joints and 162 truss elements. Among the 550 total orthotropic lattice unit cells that can be generated within this RVE, the optimal bending-dominated lattice unit cells are observed to outperform any other stretching-dominated lattice unit cells, including the Octet unit cell, under uniaxial compression. More details on the RVE and comparisons of several optimal lattice unit cells with respect to mass can be found in our previous study [20]. Numerical and experimental comparisons with bending-dominated lattice structures can be found in Section 4.1. These optimal bending-dominated unit cells can be very advantageous to serve as shape memory structures due to their strong, lightweight, and flexible bending responses. The undesired buckling phenomenon of the lattice elements can be avoided by replacing the standard cylindrical elements with biomimetic rods that have higher buckling strengths [32]. From [20], we selected different optimal bending-dominated lattice unit cells to compare them with the stretching-dominated Octet lattice structure. Fig. 4 presents the 3D printed unit cells before (left) and after (right) deformation due to uniaxial compression. Hence these unit cells are further considered for their strength and recovery stress (Refer to Table S3 for representation of 4×4 lattice cells).

In case of the thin-walled cellular unit cells, there is no classification criteria so far and the Maxwell's criterion was not applied due to the local bending and buckling behavior of the thin walls, especially in the out-of-plane orientation. But in the in-plane orientation, although the local bending or buckling of the walls are predominant, the global thin-walled unit cell might display a 2D frame like behavior. To substantiate this, we applied the 2D Maxwell's criterion for rigidity of frames (Eq. (1)) to design structures distinguished as bending-dominated and stretching-dominated thin-walled cellular unit cells by ignoring the local bending and buckling modes. Using stereolithographic additive manufacturing (Formlabs, Form 3 system) and a commercial polymer (Clear), we printed these unit cells (20 mm height, 1.5 mm wall thickness) to observe their behavior under uniaxial compression tests (Refer Table S1 for material properties). A test speed of 0.5 mm/min and uniform cell wall thickness are maintained for all the structures. Structure in Fig. 5(a) is classified as stretching-dominated as M is greater than zero based on the number of wall elements ($b = 40$) and the number of joints ($j = 21$), and the structure in Fig. 5(b) is classified as bending-dominated as M is less than 0 ($b = 24$, $j = 21$). Note that the structures in Fig. 5(a) are not optimized and only used to depict the structural

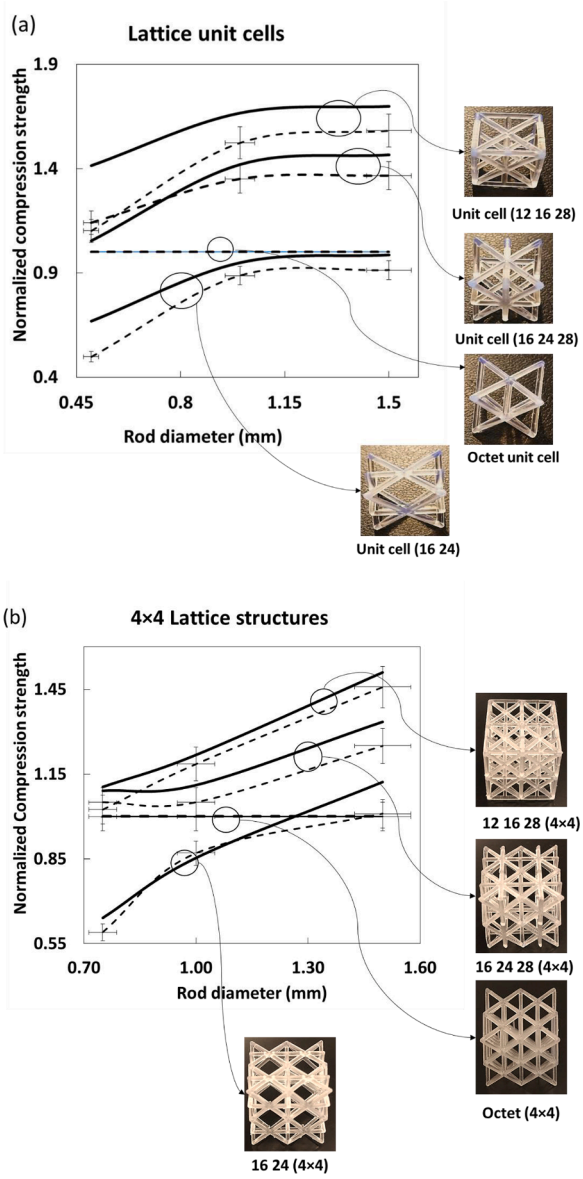

Fig. 7. Experimental (solid lines) and numerical (dashed lines) comparisons for (a) lattice unit cells, (b) 4 × 4 lattice structures under uni-axial compression test. The thin solid cross represents the error bars from experiments. The thin circle covering the numerical and experimental lines indicates that these two lines belong to the same unit cell, as indicated by the arrow. With the same overall volume, the optimal lattice unit cells (12 16 28 and 16 24 28) can be seen exhibit 10–60% higher compression strength compared to Octet unit cell in (a). The 4 × 4 lattice structures in (b) formed by using the unit cells in (a) can also be seen to follow the similar pattern as their unit cells. Here normalized compressive strength is the ratio of the compressive strength of each lattice and the compressive strength of the Octet unit cell.

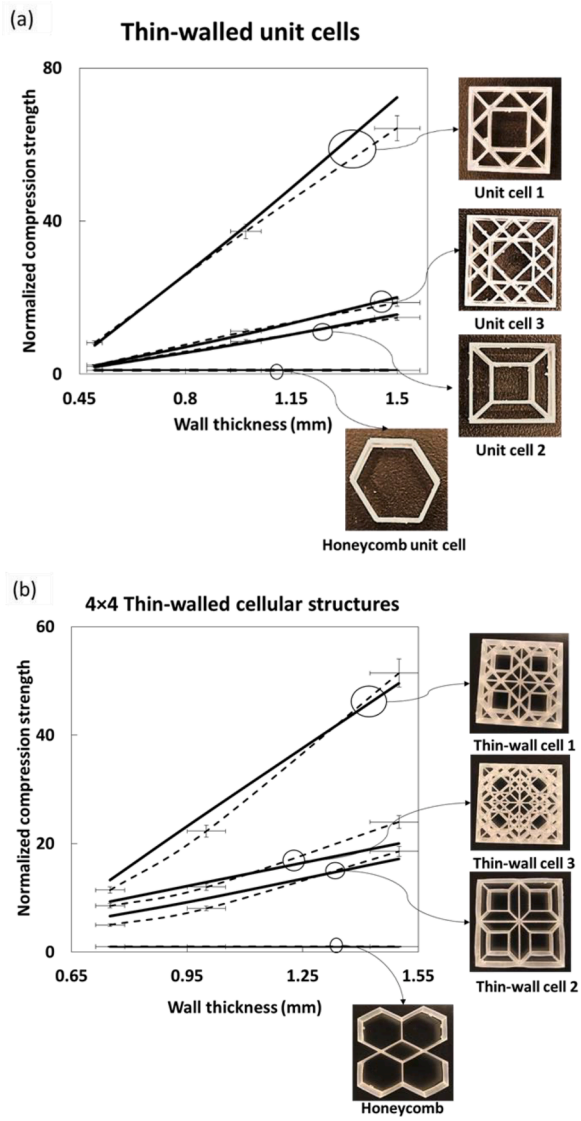

Fig. 8. Experimental (solid lines) and numerical (dashed lines) comparisons for (a) thin-walled unit cells, (b) 4 × 4 thin-walled cellular structures under uni-axial compression tests. The thin slod cross represents the error bars from experiments. The thin circle covering the numerical and experimental lines indicates that these two lines belong to the same unit cell, as indicted by the arrow. The thin-walled unit cells in (1, 2 and 3) in (a) as well as the 4 × 4 cellular structures formed using the same unit cell can be seen to exhibit much superior compression strength properties compared to honeycomb structure. The superiority of the optimal unit cells can be attributed to their higher densities and joint connectivity. The normalized compressive strength is the ratio of the compressive strength of individual thin-walled structures and the honeycomb structure.

behavior. Similar behavior can be seen in 4 × 4 cellular structures (Table S4).

From Fig. 5(a), the structure classified as stretching-dominated thin-walled structure exhibits a global stretching like behavior by fracturing at the peak load while the bending-dominated structure (Fig. 5(b)) exhibits global and local bending behavior. It can also be observed from Fig. 5(b) that the bending dominated structure lasted much longer and has higher displacement but lower load carrying capacity compared to the stretching-dominated structure (Refer to Table S3 for representation of 4 × 4 cellular structure behavior). Therefore, the bending-dominated structures satisfy the requirement for larger displacement. However, as mentioned above, the two structures in Fig. 5 are not optimized. They are used for demonstration purpose only. In this study, we will optimize the bending-dominated structures so that they will also have higher strength, in addition to higher deformability, which may lead to higher recovery stress.

Based on these experimental observations, it can be presumed that the 2D Maxwell's criterion for frames can be extended into thin-walled unit cells in the in-plane orientation to classify thin-walled structures as either bending-dominated or stretching-dominated structures. Since the Maxwell's criterion was originally proposed for pin-joined structures, the following assumptions were made to apply this criterion for thin-walled structures in the in-plane orientation: (1) Local bending or

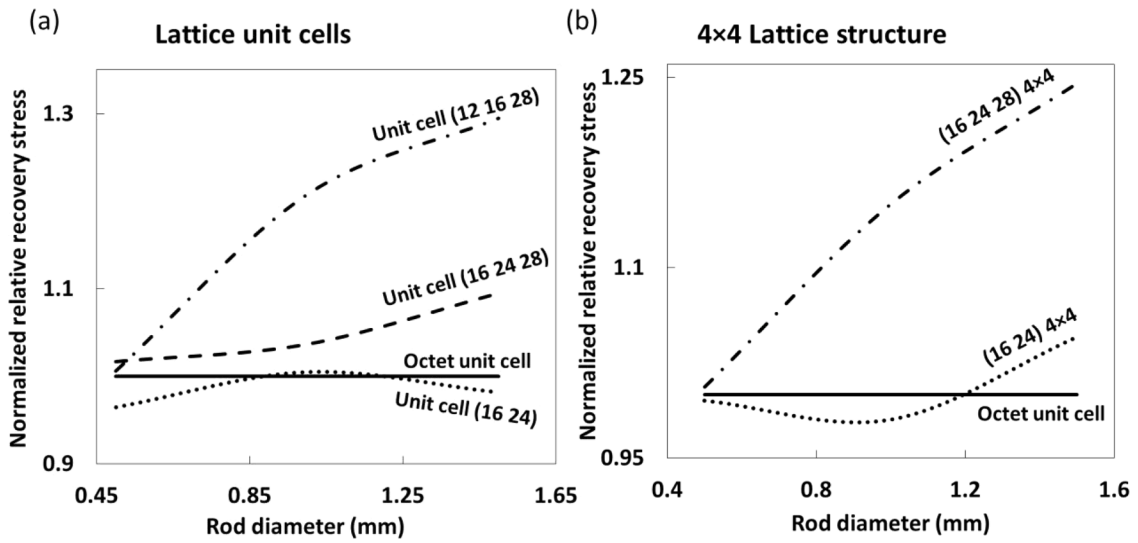

Fig. 9. Experimental comparisons for the normalized recovery stress of (a) Lattice unit cells, (b) 4 × 4 lattice structures. Here the normalized recovery stress is the ratio of specific recovery stress of each lattice unit cell and the specific recovery stress of the Octet unit cell under uniform overall volume. The lattice structures when 3D printed using a shape memory polymer, can be seen to exhibit superior (by 30%) stress recovery properties compared to the Octet unit cell.

bucking of the thin walls should be ignored. (2) The criterion should be used just as a preliminary screening approach to assess the overall structural behavior in the in-plane orientation only. Also, it should be noted that local buckling in rods is observed in bending-dominated structures as well and this buckling is caused due to overall structural bending. The buckling of rods in stretching-dominated structures, however, is due to the overall structural stretching like behavior.

Now by using this criterion and designing bending-dominated structures with higher load carrying capacities (compression strengths), optimal thin-walled unit cells that are strong as well as flexible can be created. These unit cells may lead to multifunctional applications such as high strength and high recovery stress. To mitigate the local buckling of the thin walls, we designed hybrid wall structures by mimicking giant clam seashell structures. Refer to Fig. S1 for designs and comparison on the biomimetic walls.

3.4. Inverse design framework

To design optimal thin-walled unit cells or to extract them from the vast design space created using the RVE, conventional data filtering or design extraction is cumbersome especially, when the global dataset size is huge. Though the machine learning regression models can be used to predict the structural properties with less effort, an inverse design framework that could produce or extract optimal designs much closer to the global optima is needed. Previously, we used a combination of GANs and machine learning regression models to develop an inverse design framework to create new lattice unit cells with high strength [33] and cellular unit cells with high energy absorption [21]. A GAN consists of two neural networks, a generator, and a discriminator. The duty of the generator is to generate data and feed it to the discriminator. The discriminator, which is fed with a training dataset (structural fingerprints in this context), is trained to distinguish the data from the generator into real or fake data. The real data are fingerprints similar to the training data but not exactly the same and the fake data are random noise. Now both the generator and discriminator run in a loop to train with each other (based on the training dataset fed to the discriminator) until the generator learns to only generate real data (true fingerprints). While the machine learning regression facilitates easier and faster property predictions, the GANs generate novel structures closer to the global optima. Though the GANs are proven to produce impressive results, they can involve extensive coding and training processes. Moreover, the inverse design framework using GANs developed in [21,33] needs to be iteratively run to optimize a set of inputs, leading to multiple optimization steps, and would produce a set of desirable designs rather than finding the most optimal solution within the design space. Although the design space in this study is big, it is not infinite as it is restricted to a certain boundary condition (such as the RVE, limiting the total possible designs to ~750k). Therefore, using statistical tools like correlation analysis can greatly reduce the complexity of the inverse design problem and get much closer to the global optima.

The inverse design framework for this study is constructed by combining the machine learning regression models for the unit cell property prediction and a correlation analysis to design novel optimal structures as shown in Fig. 6.

Correlation analysis is a statistical method that measures the relation between an independent variable and a dependent variable. Techniques like Spearman correlation analysis have been used previously to investigate the relation between mechanical properties and mineral, elemental content in shale (clastic sedimentary rock) [58]. Pearson correlation analysis (linear) has been used to evaluate the influence of the material variables and corresponded to the experimental result of fiber reinforced cementitious materials [59]. Correlation analysis has also been extensively used in the healthcare industry such as to find the factors from a sample patient dataset that highly influence the emergency ward utilization with 88% prediction accuracy [60]. A high correlation deduces a strong influence of the independent variable on the dependent variable. The correlation analysis in this study is used to find the key elements in a structure which are the independent variables that could influence the desired mechanical property (compression strength) which is the dependent variable. Spearman correlation which is a monotonic analysis is employed for this study due to the nonlinear data type. Spearman correlation analysis works by considering the non-parametric measure of correlation between ranks of the two variables [61,62]. The Spearman correlation coefficient (r_s) is defined as the following:

$$r_s = 1 - \frac{6\sum d_i^2}{N\left(N^2-1\right)}\ , \tag{3}$$

where d is the difference between the two ranks of each observation, and N is the number of observations.

To implement correlation analysis for the inverse design framework, 10 sub-datasets of 100 random fingerprints with their masses and compressive strengths are extracted. Correlation analysis is conducted

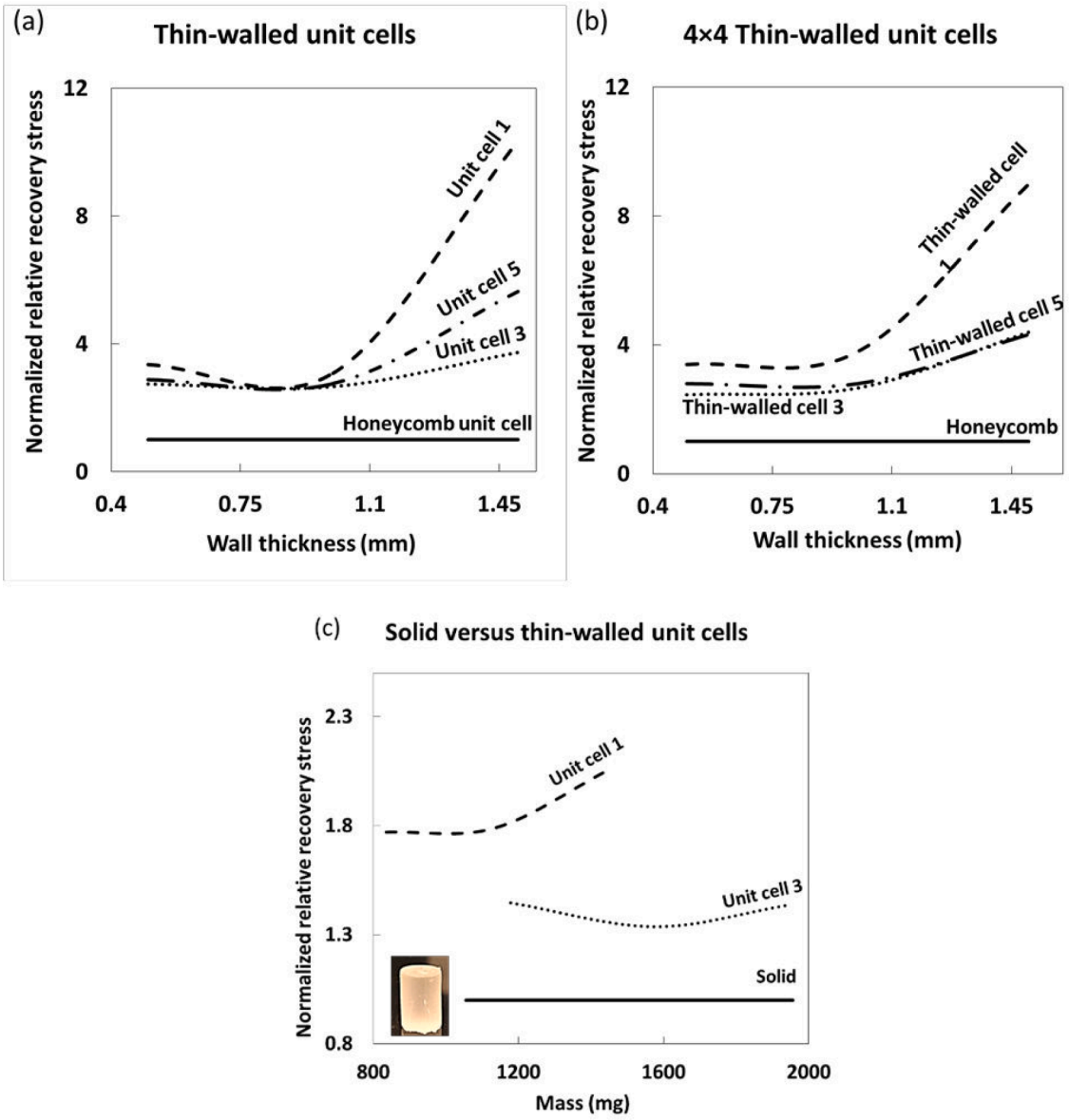

Fig. 10. Experimental comparisions for normalized recovery stress of (a) thin-walled unit cells, (b) 4 × 4 thin-walled cellular structures, and (c) thin-walled unit cell comparison with non-porous solid. Here the normalized recovery stress is the ratio of specific recovery stress of each thin-walled structure and the specific recovery stress of the honeycomb structure under uniform overall volume. Here the honeycomb structure and thin-walled unit cell 1 and unit cell 3 were categorized as bending-dominated. The thin-walled unit cell 5 is categorized as stretching-dominated. From (a) and (b), compared to the honeycomb, the optimized structures are exponentially superior in terms of normalized recovery stress. The proposed optimal bending-dominated structures both the unit cells and the 4 × 4 structures exhibit similar or even higher recovery stress properties (~50%) compared to the optimal stretching-dominated thin-walled structure.

on all the sub-datasets to find the elements (individual thin walls) that have higher influence on the relative compression strength. Those elements having highest influence (i.e., r_s close to 1) can be selected to form novel thin-walled structures. This will narrow down the optimization process and get much closer and faster to the global optima compared to GANs which would rather suggest multiple localized optimal suggestions for several iterations. The implementation of the correlation analysis on multiple subsets (10) is to validate the prediction accuracy of the framework. The final output will be novel lightweight thin-walled structures with superior strength and flexibility leading to higher recovery stress.

In this study, the design criterion is to use the correlation analysis to predict bending-dominated orthotropic thin-walled unit cells with the highest specific strength possible within the RVE. Maxwell's criterion (Eq. (1)) is used to extract bending-dominated structures (Refer to Table S5 for Maxwells criteria validations) and the forward machine learning regression models are used to predict the strength and mass properties of the designs. It can be comprehended from the RVE that to extract structures with orthotropic symmetry, the total number of elements condenses to 12. Up on conducting correlation analysis on 10 subsets, each holding 100 different fingerprints, following the above-mentioned optimization framework, it is predicted that elements 58, 15, 14, 47, 35, 26, 68, 59, 36, 25, 24, 69 have the highest correlation with the specific compression strength, and with element 58 ranked the highest and element 69 ranked the lowest for all the subsets. Now, using the first 4 (58, 15, 14, 47), 5 (58, 15, 14, 47, 35), and 7 (58, 15, 14, 47, 35, 26, 68) elements, orthotropic thin-walled unit cells as shown in the following sections are designed and evaluated. For example, the first 4 elements (58, 15, 14, 47) leads to the formation of fingerprint (14 47 12 23 15 58 56) named as "2″ in Fig. 1. Here the elements 12, 23 are by default considered to form orthotropy with 14, 47. Similarly, 56 is by default used to form orthotropic with 58. For the analytical

representation of the optimization statement, it can be perceived as

$$yfit = trainedModel.predictFcn(Corel1, Corel2 \ldots Coreln) \quad (4)$$

$$Max(Corel1, Corel2 \ldots Coreln) = globaloptima \quad (5)$$

here "yfit" is the function used to predict the mechanical properties of new fingerprints generated using correlation analysis and Corel 1, Corel 2 … Corel n were several subsets of fingerprints that were generated through correlation analysis discussed in the above paragraph. The maximum of each subset generated by the correlation analysis can be perceived as a local optimal solution until no further improvement in the mechanical properties can be achieved, which is where the optimal solution can be perceived as global optima within the dataset or RVE.

To validate the performance of this framework, we manually filtered the entire dataset using Python command prompt to hard code and extract the optimal thin-walled unit cells. It is observed that the unit cell which is bending-dominated and orthotropic in nature with the highest specific strength within the RVE is the unit cell named "1″ in Fig. 1. This unit cell is among the proposed unit cells using the optimization framework. Hence, this framework can be considered viable for this type of optimization problems.

3.5. 3D printing of cellular unit cells and lattice unit cells for experimental validations

To validate the propositions and models, we fabricated several optimal lattice unit cells (Fig. 7(a)), 4 × 4 lattice structures (Fig. 7(b)), thin-walled unit-cells (Fig. 8(a)) and 4 × 4 thin-walled cellular structures (Fig. 8(b)) using additive manufacturing. Since the goal is to finally propose structures with superior recovery stress based on their strength and flexibility, the lattice and thin-walled unit cells from the previous section are 3D printed using a shape memory polymer. All the unit cells are designed to be of uniform height and varying element diameter and wall thickness. The dimensions of the lattice unit cells are 10 × 10 × 10 mm and the thin-walled unit cells are 10 × 10 × 4 mm. The 4 × 4 lattice structures are 20 × 20 × 20 mm and the 4 × 4 thin-walled cellular structures are 40 × 40 × 10 mm. To compare the performance of the thin-walled unit cells with the bulk polymer, solid cylinders (diameter 8 mm, height 15 mm) were also 3D printed. The SMP used in this study is fabricated by combining Tris[2-(acryloyloxy) ethyl] isocyanurate (60%) and EPON 826 resin (40%). Detailed synthesizing, characterization and test results will be reported in a future study. An open material DLP (Digital Light Processing) additive manufacturing system (Bison 1000) is used to print all the structures at a printing temperature of 40 °C.

An MTS machine (QTEST 150 machine, MTS, USA) with a heating chamber is used to conduct the shape memory programming and stress recovery tests. The chamber is pre-heated to 75 °C (bulk polymer glass transition temperature about 70 °C) about 1 h before the training process to avoid erroneous readings due to the thermal expansions in the fixtures. Once the chamber is heated and ready, the samples are maintained in the chamber for 30 min to reach the rubbery state. After that, the samples are compression programed to 15% strain at a displacement rate of 0.5 mm/min. Once reaching the set strain percentage, the samples are fixed at the compressed shape by rapidly cooling down to room temperature by holding the strain constant. Once at room temperature, the load is removed to fix a temporary shape and it is observed that the shape fixity ratio (Eq. (6)) for all the structures is almost 100%. Later, the recovery stress for each sample is recorded from the load cell by reheating the samples back to 75 °C while maintaining zero recovery strain.

$$F = \frac{\varepsilon_f}{\varepsilon_l} \times 100\% \quad (6)$$

where ε_f is the fixed strain after load removal and ε_l is the measured strain before load removal.

4. Results

The optimal lightweight cellular unit cells proposed using the inverse design framework in the previous sections along with the lattice unit cells extracted from [21, 32] were modeled and 3D printed for numerical and experimental validations. Section 4.1 presents the numerical and experimental validations for several thin-walled and lattice structures with both unit cells and 4 × 4 structures under uni-axial compression. Section 4.2 discusses the shape memory performance of the same 3D printed structures using a shape memory polymer ink, and their comparison with Octet and honeycomb structures.

4.1. Model validation

Numerical comparisons using ANSYS simulation tool along with the experimental validations are presented in Fig. 7 for lattice structures and Fig. 8 for thin-walled cellular structures. The proposed lattice structures, while are still bending-dominated, can be seen to exhibit similar or ever better relative compression strength properties compared to the classic Octet truss structure which is stretching-dominated in nature. In Fig. 7, it should be noted that the comparisons were made with respect to the rod diameters of the lattice structures. Many studies prove that the performance of lattice structures is vastly dependent on their relative densities [35,55,56,63,64]. While the intention of Fig. 7 is to give a normalized comparison over rod diameters, comparisons for the same optimal lattice structures with Octet structures over relative densities were discussed previously in [20,33]. With respect to relative densities, the optimal lattice unit cells rendered in this study still exhibit superior specific compression strength properties.

The optimal thin-walled unit cells in Fig. 8(a) can also be seen to be exceptionally superior to honeycomb unit cell in terms of compressive strength (in-plane orientation). These unit cells due to their local and global bending like behavior will possess flexibility or larger displacements as demonstrated in Fig. S3.

It can also be observed that the 4 × 4 lattice in Fig. 7(b) and cellular structures in Fig. 8(b) exhibit similar properties to that of their unit cells. Refer to Fig. S4 for comparisons with densities for thin-walled unit cells.

4.2. Shape memory analysis for optimal lightweight structures

The comparisons for the optimal lattice unit cells with Octet lattice, the proposed thin-walled unit cells with honeycomb unit cell, and the thin-walled unit cell with the solid samples are presented in Figs. 9 and 10 respectively.

As can be seen from Fig. 9(a) and (b), the optimal bending-dominated lattice unit cells and 4 × 4 lattice structures, especially unit cell (12 16 28) and unit cell (16 24 28) have about 10–30% higher specific recovery stress (recovery stress/overall volume) compared to Octet unit cell with the same lattice member dimeter.

From Fig. 10(a) and (b), the recovery stress of the optimal thin-walled unit cells and 4 × 4 cellular structures (unit cell 1 and unit cell 3) are 200–1000% more than that of the honeycomb unit cell; their recovery stress is also 50% more than that of an optimal stretching-dominated (unit cell 5) structure (Refer to Fig. S5 for 3D printed sample images, and Fig. S8 for recovery stress versus density comparisons). Fig. 10(c) shows the comparisons of the mass normalized recovery stress of the optimal thin-walled unit cells and solid material with varying mass, and the optimal unit cells can be seen to exhibit 140–200% higher recovery stress than the solid structure. It should be noted that the Octet lattice unit cell and 4 × 4 × 4 Octet lattice structure are stretching-dominated in nature. The optimized lattice unit cells are bending-dominated in behavior. The optimized 4 × 4 × 4 lattice structures, which are either bending-dominated or partially bending-dominated, also exhibit superior recovery stress compared to Octet unit cell and 4 × 4 × 4 Octet lattice structure. Similarly, the optimized thin-walled unit cells and 4 × 4 × 4 cellular structures, despite being bending-dominated,

still exhibit better recovery stress compared to their stretching-dominated counterparts. This shows that the bending-dominated unit cells can be potential candidates with multifunctional capabilities like superior strength, flexibility, and shape memory.

Also, since the optimization process is based on the structural behavior of the unit cells only, it should be noted that using different SMPs would influence their structural performance and shape memory effect. In this study, the SMP used is brittle in nature (at room temperature) which could lead to less overall displacements before fracture. A more ductile SMP can improve the range of displacements when training or programming the structures. A more ductile SMP may also need to consider the nonlinear behavior and viscoelasticity and viscoplasticity during our finite element modeling to create the training dataset. In this study, because all the lattice unit cells and thin-walled cellular unit cells used the same brittle SMP in our modeling and experiments, it is believed that the conclusions may not be changed should another ductile SMP be used.

5. Conclusions

Lightweight lattice unit cells and thin-walled cellular unit cells for superior shape memory properties are explored. A novel inverse design framework by combining machine learning and correlation analysis models is proposed to optimize the thin-walled unit cells. Maxwell's criterion for rigidity of frames is employed to distinguish lattice unit cell behavior and further extended into the thin-walled unit cells with certain assumptions. The optimized lightweight lattice unit cells and thin-walled unit cells exhibit excellent strong and flexible properties.

Especially, from the numerical and experimental analysis under uniaxial loading, it is observed that the stretching-dominated unit cells have higher toughness and fail due to element stretching or buckling or fracture while the bending-dominated unit cells are flexible and fail primarily due to rod bending, confirming the previous studies. Due to the element bending phenomenon, previous studies suggested that the bending-dominated structures have one third strength as compared to stretching-dominated structures. Contrary to this statement, bending-dominated unit cells with optimal joint connectivity and element orientation exhibit 60% higher relative compression strength compared to the classic Octet unit cells and most of the stretching-dominated unit cells within their RVE (Fig. 7).

The Maxwell's criterion for rigidity of frames is extended to classify thin-walled structures by ignoring the local bending (or buckling) of thin walls. This aided in the selection criteria for optimal bending-dominated thin-walled unit cells. The proposed bending-dominated lattice unit cells have 30% higher recovery stress over Octet lattice unit cell which is stretching-dominated in behavior. Using the inverse design framework based on Spearman correlation analysis and machine learning regression models, the proposed thin-walled unit cells have up to 1000% better normalized specific recovery stress compared to the honeycomb unit cell in the in-plane direction. As compared to the bulk polymer, the thin-walled unit cells show up to 200% higher specific recovery stress (Fig. 10). These unit cells follow similar trends in terms of compression strength which is used as the selection criterion for optimal recovery stress properties. The proposed bending-dominated unit cells exhibit superior load carrying, recovery stress and energy absorption properties due to their flexible nature. The proposed optimization framework can be extended to predict structures with any desired mechanical properties if enough data and control parameters are provided.

It should be mentioned that lightweight structures, especially lattice structures could undergo a complex mode of deformation including stretching, buckling, or bending, and it is vastly dependent on the rod aspect ratios. While Maxwell's criterion can be considered for preliminary screening, a thorough evaluation on the lattice behavior under various loading conditions and their failure modes must be investigated for proper understanding of their structural behavior. One limitation in this study by employing Maxwell's criterion and bending-dominated structures could cause the neglection of a few stretching-dominated structures with higher strength and deformations. Also, some lattice structures that are beyond Maxwell's criterion might be missed in this study [65,66].

Supporting information

All other data are available from the authors upon reasonable request.

CRediT authorship contribution statement

Adithya Challapalli: Visualization, Data curation, Formal analysis, Writing – original draft. **John Konlan:** Visualization. **Guoqiang Li:** Conceptualization, Funding acquisition, Investigation, Writing – original draft.

Declaration of Competing Interest

The authors declare no conflict of interest.

Data availability

Data will be made available on request.

Acknowledgments

This work is supported by the US National Science Foundation under Grant Number OIA-1946231 and the Louisiana Board of Regents for the Louisiana Materials Design Alliance (LAMDA), and National Science Foundation under grant number HRD-1736136.

Supplementary materials

Supplementary material associated with this article can be found, in the online version, at doi:10.1016/j.ijmecsci.2022.108029.

References

[1] Tibbits S. 4D printing: multi-material shape change. Archit Des 2014;84:116–21.
[2] Khoo ZX, Teoh JEM, Liu Y, Chua CK, Yang S, An J, Leong KF, Yeong WY. 3D printing of smart materials: a review on recent progresses in 4D printing. Virtual Phys Prototyp 2015;10:103–22.
[3] Regehly M, Garmshausen Y, Reuter M, et al. Xolography for linear volumetric 3D printing. Nature 2020;588:620–4.
[4] Kelly BE, Bhattacharya I, Heidari H, Shusteff M, Spadaccini C, Taylor H. Volumetric additive manufacturing via tomographic reconstruction. Science 2019;363:1075–9.
[5] Liu Y, Du H, Liu L, Leng J. Shape memory polymers and their composites in aerospace applications: a review. Smart Mater Struct 2014;23:023001.
[6] Lan X, Liu Y, Lv H, Wang X, Leng J, Du S. Fiber reinforced shape-memory polymer composite and its application in a deployable hinge. Smart Mater Struct 2009;18:024002.
[7] Li G, Nettles D. Thermomechanical characterization of a shape memory polymer based self-repairing syntactic foam. Polymer 2010;51:755–62.
[8] Li G, Uppu N. Shape memory polymer based self-healing syntactic foam: 3-D confined thermomechanical characterization. Compos Sci Technol 2010;70:1419–27.
[9] Lai SM, Lan YC. Shape memory properties of melt-blended polylactic acid (PLA)/thermoplastic polyurethane (TPU) bio-based blends. J Polym Res 2013;20:140.
[10] Soleyman E, et al. Smart Mater Struct 2022;31:085002.
[11] Hashmi SAR, Prasad HC, Abishera R, Bhargaw HN, Naik A. Improved recovery stress in multi-walled-carbon-nanotubes reinforced polyurethane. Mater Des 2015;67:492–500.
[12] Koerner H, Price G, Pearce NA, Alexander M, Vaia RA. Remotely actuated polymer nanocomposites—Stress-recovery of carbon-nanotube-filled thermoplastic elastomers. Nat Mater 2004;3:115.
[13] Fan J, Li G. High enthalpy storage thermoset network with giant stress and energy output in rubbery state. Nat Commun 2018;9:642.
[14] Feng X, Li G. High-temperature shape memory photopolymer with intrinsic flame retardancy and record-high recovery stress. Appl Mater Today 2021;23:101056.
[15] Keshavarzan M, Kadkhodaei M, Forooghi F. An investigation into compressive responses of shape memory polymeric cellular lattice structures fabricated by vat polymerization additive manufacturing. Polym Test 2020;91:106832.

[16] Li A, Challapalli A, Li G. 4D printing of recyclable lightweight architectures using high recovery stress shape memory polymer. Sci Rep 2019;9:7621.
[17] Silva MJ, Gibson LJ. The effects of non-periodic microstructure and defects on the compressive strength of two-dimensional cellular solids. Int J Mech Sci 1997;39(5): 549–63.
[18] Challapalli A, Ju J. Continuum model for effective properties of orthotropic octet-truss lattice materials. In: Proceedings of the ASME International Mechanical Engineering Congress and Exposition; 2014.
[19] Wen C, Seth W, Julie AJ, William LS, Daniel AT, Christopher MS. Stiff isotropic lattices beyond the Maxwell criterion. Sci Adv 2019;5:9.
[20] Challapalli A, Li G. Machine learning assisted design of new lattice core for sandwich structures with superior load carrying capacity. Sci Rep 2021;11:18552.
[21] Challapalli A, Konlan J, Patel D, Li G. Discovery of cellular unit cells with high natural frequency and energy absorption capabilities by an inverse machine learning framework. Front Mech Eng 2021;7:779098.
[22] Yang C, Boorugu M, Dopp A, Ren J, Martin R, Han D, Choi W, Lee H. 4D printing reconfigurable, deployable and mechanically tunable metamaterials. Mater Horiz 2019;6:1244–50.
[23] Ming L, Wei H, Zeang Z, Craig H, Mingji C, Haibao L, Jerry H. 3D printing of auxetic metamaterials with digitally reprogrammable shape. ACS Appl Mater Interfaces 2019;11:22768–76.
[24] Berwind MF, Kamas A, Eberl C. A hierarchical programmable mechanical metamaterial unit cell showing metastable shape memory. Adv Eng Mater 2018;20: 1800771.
[25] Matheus BF, Luiz JP, Guilherme AO, Lucas RS, Sebastião SC, Guilherme FG. A review on the energy absorption response and structural applications of auxetic structures. Mech Adv Mater Struct 2021:1537–6494.
[26] Matheus BF, Luiz JP, Guilherme AO, Sebastião SC, Guilherme FG. Multi-objective design optimization of double arrowhead auxetic model using Lichtenberg algorithm based on meta-modelling. Structures 2022;45:1199–211.
[27] Xing Z, Hongling Y, Nan W, Ran T, Zhen L. Design optimization of multifunctional metamaterials with tunable thermal expansion and phononic bandgap. Mater Des 2021;209:109990.
[28] Gao C, Min X, Fang M, Tao T, Zheng X, Liu Y, Wu X, Huang Z. Innovative materials science via machine learning. Adv Funct Mater 2021;32:2108044.
[29] Gandhi A, Faruque Hasan MM. Machine learning for the design and discovery of zeolites and porous crystalline materials. Curr Opin Chem Eng 2022;35:100739.
[30] Cheng B, Du J, Yao Y. Machine learning methods to assist structure design and optimization of Dual Darrieus Wind Turbines. Energy 2022;244:122643.
[31] Ma W, Xu Y, Xiong B, Deng L, Peng RW, Wang M, Liu Y. Pushing the limits of functionality-multiplexing capability in metasurface design based on statistical machine learning. Adv Mater 2022;34:2110022.
[32] Challapalli A, Li G. 3D printable biomimetic rod with superior buckling resistance designed by machine learning. Sci Rep 2020;10:20716.
[33] Challapalli A, Patel D, Li G. Inverse machine learning framework for optimizing lightweight metamaterials. Mater Des 2021;208:109937.
[34] Ju J, Summers JD. Compliant hexagonal periodic lattice structures having both high shear strength and high shear strain. Mater Des 2011;32:512–24.
[35] Evans AG, Hutchinson JW, Ashby MF. Multifunctionality of cellular metal systems. Prog Mater Sci 1998;43:171–221.
[36] Heo H, Ju J, Kim D. Compliant cellular structures: application to a passive morphing airfoil. Compos Struct 2013;106:560–9.
[37] Zhang P, Heyne MA, To AC. Biomimetic staggered composites with highly enhanced energy dissipation: modeling, 3D printing, and testing. J Mech Phys Solids 2015;83:285–300.
[38] Panda B, Leite M, Biswal BB, Niu X, Garg A. Experimental and numerical modelling of mechanical properties of 3D printed honeycomb structures. Measurement 2018; 116:495–506.
[39] Yang K, Sun Y, Yao Y, Zhu W. A universal strategy for flexible, efficient, and programmable crashworthiness under quasi-static and dynamic loadings based on plastic deformation of metals. Mater Des 2022;222:111027.
[40] Zhang Y, Wang Q, Tichem M, et al. Design and characterization of multi-stable mechanical metastructures with level and tilted stable configurations. Extrem. Mech Lett 2020;34:100593.
[41] Huang Y, Wu D, Chen M, Zhang K, Fang D. Evolutionary optimization design of honeycomb metastructure with effective mechanical resistance and broadband microwave absorption. Carbon 2021;177:79–89.
[42] Sui N, Yan X, Huang TY, Xu J, Yuan FG, Jing Y. A lightweight yet sound-proof honeycomb acoustic metamaterial. Appl Phys Lett 2015;106:171905.
[43] Zhang Y, Gao L, Xiao M. Maximizing natural frequencies of inhomogeneous cellular structures by kriging-assisted multiscale topology optimization. Comput Struct 2020;230:106197.
[44] Tsang HH, Raza S. Impact energy absorption of bio-inspired tubular sections with structural hierarchy. Compos Struct 2018;195:199–210.
[45] Desguers T, Robinson A. Thermal analysis of evacuated honeycomb structures: experimental validation and optimization of non-uniform structures. Int J Heat Mass Transf 2022;196:123249.
[46] Ju J, Kim DM, Kim K. Flexible cellular solid spokes of a non-pneumatic tire. Compos Struct 2012;94:2285–95.
[47] Lendlein A, Kelch S. Shape memory polymers. Angew Chem Int Ed 2002;41: 2034–57.
[48] Li G, Xu W. Thermomechanical behavior of thermoset shape memory polymer programmed by cold-compression: testing and constitutive modeling. J Mech Phys Solids 2011;59:1231–50.
[49] Yan C, Li G. Design oriented constitutive modeling of amorphous shape memory polymers, and its application to multiple length scale lattice structures. Smart Mater Struct 2019;28:095030.
[50] Yang Q, Li G. Temperature, and rate dependent thermomechanical modeling of shape memory polymers with physics-based phase evolution law. Int J Plast 2016; 80:168–86.
[51] Li G, Shojaei A. A viscoplastic theory of shape memory polymer fibers with application to self-healing materials. Proc R Soc Math Phys Eng Sci 2012;468: 2319–46.
[52] Li G, Wang A. Cold, warm, and hot programming of shape memory polymers. J Polym Sci Part B Polym Phys 2016;54:1319–39.
[53] Sha Y, Jiani L, Haoyu C, Robert OR, Jun X. Design and strengthening mechanisms in hierarchical architected materials processed using additive manufacturing. Int J Mech Sci 2018;149:150–63.
[54] Tan XP, Tan YJ, Chow CSL, Tor SB, Yeong WY. Metallic powder-bed based 3D printing of cellular scaffolds for orthopedic implants: a state-of-the-art review on manufacturing, topological design, mechanical properties, and biocompatibility. Sci Eng C 2017;76:1328–43.
[55] Maxwell JC. On the calculation of the equilibrium and stiffness of frames. Philos Mag 1864;27:294.
[56] Deshpande VS, Fleck NA, Ashby MF. Foam topology bending vs stretching dominated architecture. Acta Mater 2001;49:1035–40.
[57] Deshpande VS, Fleck NA, Ashby MF. Effective properties of the octet-truss lattice material. J Mech Phys Solids 2001;49:1747–69.
[58] Gang Z, Wenlong D, Jing T, Jingshou L, Yang G, Siyu S, Ruyue W, Ning S. Spearman rank correlations analysis of the elemental, mineral concentrations, and mechanical parameters of the Lower Cambrian Niutitang shale: a case study. J Pet Sci Eng 2022;208(Part C):109550.
[59] Lin WT, Wu YC, Cheng A, Chao SJ, Hsu HM. Engineering properties and correlation analysis of fiber cementitious materials. Materials 2014;7:7423–35.
[60] Tummala, R., Predictive modeling of FMOL health system utilization using machine learning algorithms and retrospective study of COVID tested patients, LSU Master's Theses. (2021).
[61] Chengwei X, Jiaqi Y, Rui ME, Chunming R. Using Spearman's correlation coefficients for exploratory data analysis on big dataset. Concurr Comput Pract Exp 2016;28:3866–78.
[62] Bonett DG, Wright TA. Sample size requirements for estimating pearson, kendall and spearman correlations. Psychometrika 2000;65:23–8.
[63] Boniotti L, Beretta S, Patriarca L, Rigoni L, Foletti S. Experimental and numerical investigation on compressive fatigue strength of lattice structures of AlSi7Mg manufactured by SLM. Int J Fatigue 2019;128:105181.
[64] Favre J. A continuous crystallographic approach to generate cubic lattices and its effect on relative stiffness of architectured materials. Addit Manuf 2018;21: 359–68.
[65] Chen W, Watts S, Jackson JA, Smith WL, Tortorelli DA, Spadaccini CM. Stiff isotropic lattices beyond the Maxwell criterion. Sci Adv 2019;5:1937.
[66] Lai CQ, Markandan K, Lu Z. Anomalous elastic response of a 3D anti – tetra-chiral metamaterial. Int J Mech Sci 2021;192:106142.